Orbital origin of the electrical conduction in ferromagnetic atomic-size contacts: Insights from shot noise measurements and theoretical simulations

R. Vardimon,[1,*] M. Matt,[2] P. Nielaba,[2] J. C. Cuevas,[3] and O. Tal[1]

[1]*Department of Chemical Physics, Weizmann Institute of Science, Rehovot 76100, Israel*

[2]*Department of Physics, University of Konstanz, D-78457 Konstanz, Germany*

[3]*Departamento de Física Teórica de la Materia Condensada and Condensed Matter Physics Center (IFIMAC), Universidad Autónoma de Madrid, E-28049 Madrid, Spain*

(Received 8 December 2015; published 29 February 2016)

With the goal of elucidating the nature of spin-dependent electronic transport in ferromagnetic atomic contacts, we present here a combined experimental and theoretical study of the conductance and shot noise of metallic atomic contacts made of the 3*d* ferromagnetic materials Fe, Co, and Ni. For comparison, we also present the corresponding results for the noble metal Cu. Conductance and shot noise measurements, performed using a low-temperature break-junction setup, show that in these ferromagnetic nanowires, (i) there is no conductance quantization of any kind, (ii) transport is dominated by several partially open conduction channels, even in the case of single-atom contacts, and (iii) the Fano factor of large contacts saturates to values that clearly differ from those of monovalent (nonmagnetic) metals. We rationalize these observations with the help of a theoretical approach that combines molecular dynamics simulations to describe the junction formation with nonequilibrium Green's function techniques to compute the transport properties within the Landauer-Büttiker framework. Our theoretical approach successfully reproduces all the basic experimental results and it shows that all the observations can be traced back to the fact that the *d* bands of the minority-spin electrons play a fundamental role in the transport through ferromagnetic atomic-size contacts. These *d* bands give rise to partially open conduction channels for any contact size, which in turn lead naturally to the different observations described above. Thus, the transport picture for these nanoscale ferromagnetic wires that emerges from the ensemble of our results is clearly at variance with the well established conduction mechanism that governs the transport in macroscopic ferromagnetic wires, where the *d* bands are responsible for the magnetism but do not take part in the charge flow. These insights provide a fundamental framework for ferromagnetic-based spintronics at the nanoscale.

DOI: 10.1103/PhysRevB.93.085439

I. INTRODUCTION

When the characteristic dimensions of a metallic wire are shrunk all the way down to the atomic scale, its electronic transport properties change dramatically as a consequence of the appearance of quantum mechanical effects. This has been nicely illustrated in recent years with the help of metallic atomic contacts fabricated by means of scanning tunneling microscopes (STMs) and break-junction techniques [1]. Thus for instance, it has been shown that transport properties such as the conductance [1,2], shot noise [3–8], or thermopower [9–11] differ markedly from those of macroscopic wires, while transport phenomena such as Joule heating [12,13] or magnetoresistive effects [14–19] take place in a very different manner in these nanowires. In all cases, these dramatic differences can be traced back to the fact that the transport in metallic atomic contacts is mainly quantum coherent. The central goal of this work is to show that the nature of electrical conduction in ferromagnetic atomic contacts is clearly at variance with the established picture in macroscopic wires.

Our present understanding of electrical conduction in macroscopic wires made of ferromagnetic metals such as Fe, Co, and Ni is largely based on the semiclassical model put forward by Mott in the 1930s [20,21]. In that simple model, sometimes referred to as the two-current model, the current is carried by the electrons of two independent spin bands, the majority-spin electrons and the minority-spin electrons. Moreover, it is assumed that the conduction bands have an *s* character, while the *d* electrons are localized and the corresponding spin-split bands are responsible for the net magnetization. Mott described the conductivity of a ferromagnetic metal in terms of the Drude formula, where the key parameters are the density of conduction electrons, assumed to be spin-independent, and the spin-dependent inelastic scattering time (or relaxation time). While the relaxation time for the majority-spin electrons is similar to that of a nonmagnetic metal, the scattering of minority-spin electrons from the *s* states into the partially occupied *d* states reduces considerably the corresponding relaxation time and, in turn, the electrical conductivity in ferromagnetic metals. This explains, for instance, why Fe, Co, and Ni are less conductive than the noble metals (Au, Ag, and Cu). Moreover, this model predicts that the conduction is dominated by the majority-spin electrons, leading to a positive spin polarization of the current. This simple picture turns out to be quite accurate, as has been very recently demonstrated using ultrafast terahertz spectroscopy [22]. However, as we shall show in this work, it severely fails to explain the transport properties in ferromagnetic atomic contacts.

Since the advent of STM-based and break-junction techniques in the 1990s, many experimental studies of transport through atomic contacts made of ferromagnetic metals have been reported [14–19,23–50]. Some of the early reports focused on the observation of half-integer quantization, i.e., on the observation of peaks in the conductance histograms at half-integer multiples of the quantum of conductance

*Corresponding author: rvardimon@gmail.com

$G_0 = 2e^2/h$ [15,34–39]. In the Landauer picture of the coherent transport through these ferromagnetic nanowires, the low-temperature linear conductance is given by $G = (G_0/2)\sum_{n,\sigma}\tau_{n,\sigma}$, where $\tau_{n,\sigma}$ is the transmission coefficient at the Fermi energy of the nth available conduction channel for a spin σ. Thus, these observations were interpreted as evidence indicating that only spin-split fully open channels contribute to the conductance in these atomic-scale ferromagnetic wires. This interpretation was questioned by Untiedt *et al.* [40], who measured the conductance for atomic contacts of Fe, Co, and Ni using break junctions under cryogenic vacuum conditions. Contrary to the experiments mentioned above, they reported the absence of fractional conductance quantization. Instead, they observed conductance histograms that show broad peaks above $1G_0$. Moreover, they suggested that the observation of peaks in the conductance histograms at half-integer values of G_0 could be due to contamination. We note that half-integer conductance values are occasionally detected for arbitrarily realized atomic-scale contacts of both ferromagnetic and nonferromagnetic metals.

Another controversy in the context of ferromagnetic atomic contacts has to do with the observation of an anomalous anisotropic magnetoresistance (AMR). AMR is a spintronic effect in which the resistance varies as a function of the relative orientation between the magnetization and the current directions and it originates from spin-orbit interaction. Bolotin *et al.* [14] reported that the magnitude of the AMR of permalloy atomic contacts can be considerably larger than in bulk samples and that it exhibits an anomalous angular dependence. Similar observations were reported by Viret *et al.* [46] in Fe contacts, but they also reported the occurrence of conductance jumps upon the rotation of the magnetization. Similar stepwise variations in the conductance were later found in Co nanocontacts [15]. These jumps were tentatively interpreted as a manifestation of the so-called ballistic AMR (BAMR) [51]. This approach suggested that in a ballistic contact the rotation of the magnetization could result in variations in band crossing at the Fermi energy, leading to an abrupt change in the conductance on the order of $G_0/2$. However, as discussed above, ferromagnetic contacts are not expected to be ballistic (i.e., to exhibit only fully open channels), and therefore, the interpretation in terms of BAMR is highly questionable [52]. In fact, Shi and Ralph [53] suggested that these jumps might originate from sudden atomic rearrangements [54].

Half-integer quantization and BAMR are not inherently expected in ferromagnetic atomic contacts in view of the established picture of the conduction in these atomic-scale wires [2,55]. Within this picture, based on the Landauer approach to coherent transport, the conduction channels in a nonmagnetic metal are spin degenerate and are determined by the orbital structure of the metal and the geometry of the atomic contact. In particular, the number of conduction channels of a single-atom contact is expected to be limited by the number of valence orbitals, as was experimentally verified with the use of superconductivity to extract the channel content [2]. Moreover, it was established that conductance quantization is only expected in few-atom contacts of monovalent metals, whereas in the case of multivalent metals the conductance is essentially determined by several partially open channels and there are no signs of conductance quantization.

The controversies discussed above and the great interest in spin-dependent transport at the nanoscale have led numerous theoretical groups to investigate the transport properties of ferromagnetic atomic contacts [51,52,56–82]. Apart from the analysis of the conductance and the AMR, these studies have also addressed many different aspects of the physics of these contacts such as the electronic structure of ideal systems, such as monoatomic wires, the influence of domain walls on electronic and transport properties, or the magnetic structure. The ensemble of the reported theoretical results clearly suggests that the d orbitals play a fundamental role in the transport properties of these atomic-scale wires, contrary to their macroscopic counterparts, and there is no fundamental reason for expecting either conductance quantization or full spin polarization. However, there is still no generally accepted picture for electrical conduction in ferromagnetic atomic contacts for two main reasons. First, a systematic one-to-one comparison between experiment and theory for the conductance has never been established. This is a difficult task since it requires from the theory side obtaining a simultaneous description of the detailed atomic structure and transport properties of the contact. Second and more important, transport measurements performed so far in ferromagnetic atomic contacts have been restricted to the conductance, which does not contain information about the individual transmission coefficients. The access to this information was the key breakthrough that finally enabled elucidating the nature of the conduction in nonmagnetic atomic contacts, something that became possible thanks to the use of superconductivity [2,83]. However, such a method is not possible in the case of ferromagnetic contacts.

In this work we revisit the nature of the electrical conduction in ferromagnetic atomic contacts by providing a very detailed experimental study of both conductance and shot noise in Fe, Co, and Ni atomic contacts at cryogenic temperature and vacuum conditions. We present the corresponding results for Cu contacts for comparison. In particular, we show how shot noise measurements provide an insight into the electrical conduction of these ferromagnetic nanowires, which is crucial to understand how they differ from nonmagnetic atomic-scale contacts and macroscopic ferromagnetic wires. Moreover, we supplement our experimental study with a comprehensive theoretical analysis based on molecular dynamics (MD) and quantum mechanical calculations of the transport properties that allows us to establish a direct comparison with our experiments for the different materials under study. From the experimental side, our main results for the ferromagnetic contacts are (i) the confirmation of the lack of any kind of conductance quantization, (ii) we find no signs of pronounced shot noise suppression at any conductance value, contrary to noble metals, which shows that the transport is dominated by partially open channels for any contact size, (iii) the analysis of shot noise shows that at least several channels contribute to transport even in smallest (presumably one-atom) contacts, again in clear contrast with noble metals, and (iv) the Fano factor saturates for contacts with conductances higher than $10G_0$ to a value that is clearly larger than for monovalent metals. Our theoretical results reproduce very satisfactorily all these basic observations. In all cases, the origin of these observations can be traced back to the fact that the $3d$ orbitals play a major role in the conduction of these ferromagnetic atomic contacts.

The picture that emerges is that in a ferromagnetic contact the majority-spin electrons behave as in a noble metal, where the conduction is dominated by the *s* conduction band, while the minority-spin electrons behave as in a transition metal, where both *s* and *d* orbitals contribute decisively to the transport properties. In particular, the *d* orbitals corresponding to the minority-spin bands build up partially open channels which, in turn, are responsible for the experimental observations described above. Moreover, these additional conduction channels are responsible for the higher conductance of ferromagnetic few-atom contacts as compared with noble metals and they give rise to a negative spin polarization of the current in all three ferromagnetic 3*d* metals, in clear contrast to the positive spin polarization in macroscopic wires. Thus, our study provides a consistent general picture of the conduction in ferromagnetic atomic contacts and their unique transport properties compared to macroscopic ferromagnetic wires.

The rest of the paper is organized as follows. In Sec. II we describe the experimental and theoretical techniques that we have used to investigate both the conductance and the shot noise of ferromagnetic atomic contacts. We present in Sec. III our results for the conductance histograms of the different materials studied in this work. Section IV is devoted to the description of our experimental and theoretical results for the shot noise and Fano factor. We present a detailed discussion on the origin of our results in terms of the nature of the conduction channels in Sec. V. Section VI is devoted to further discussion of our results. Then, we summarize our main conclusions in Sec. VII. Finally, in the Appendix we show the results for Co and Fe that are not presented in the main text.

II. GENERAL METHODOLOGY

In this section we describe the basic experimental and theoretical methods that we have employed in this work to study both the conductance and shot noise of ferromagnetic atomic contacts.

A. Experimental techniques

Our measurements were performed using a mechanical controllable break junction (MCBJ) [84] composed of a notched metal wire attached to a flexible substrate (see Fig. 1). The wires used consist of a high-purity metal ($\geqslant$99.9%) and have macroscopic dimensions (0.1 mm diameter). The sample is positioned in a vacuum chamber that is initially pumped to $\sim 10^{-5}$ mbar and cooled by liquid helium to $\sim$4.2 K. Once the sample is cold, a mechanical push screw is used to bend the substrate until the wire breaks in its weakest spot, forming two atomically sharp tips. Since the junction is held under cryogenic vacuum, the freshly exposed tips are kept with minimum exposure to impurities. This is extremely important to avoid oxidation or other contaminations, which can have a considerable effect on transport [19,40]. The displacement between the tips is then controlled with sub-Ångström resolution by the precise movement of a piezoelectric element. The tips can be pushed back towards each other to reform an atomic contact, whose minimal cross section can be varied by changing the voltage applied on the piezo element.

The electronic conductance across the atomic contact is measured by connecting measurement wires to the two sides of the thinned metallic wire, which essentially serve as leads to the atomic-scale junction. Figure 1 shows the electronic circuit used for conductance and shot noise measurements. Two computer-controlled relays are used to toggle between conductance (marked in red) and noise (blue) measurement modes. For dc conductance measurement, a bias voltage is provided to the junction from a differential voltage source. The response current is amplified with a current preamplifier (SR 570) and recorded by a 24-bit digitizer (NI 4461). The ac conductance measurements are performed by driving a small sinusoidal signal (2 mVpp, $\sim$3 kHz) added to the bias voltage. The differential conductance dI/dV is obtained using the lock-in technique, performed digitally with the data acquisition software.

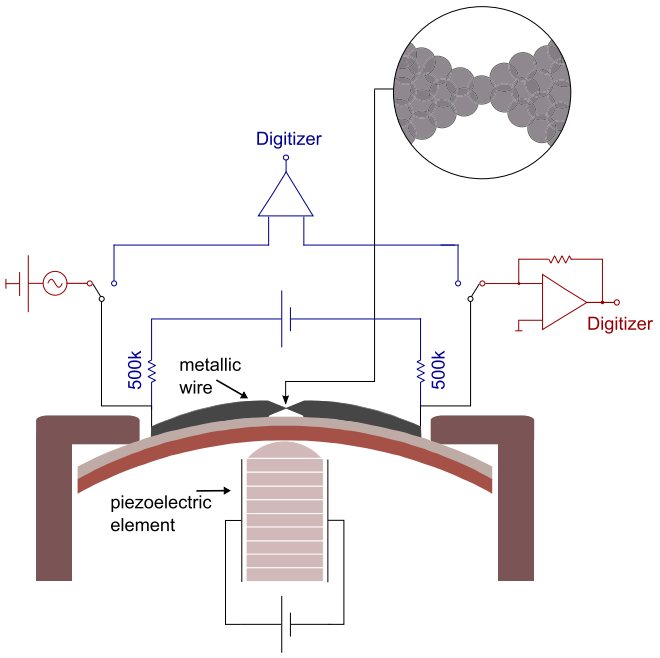

FIG. 1. Schematics of a mechanical controllable break junction setup adjusted for shot noise measurements. A notched metallic wire is broken in a controllable fashion using a piezoelectric element, allowing the formation of an atomic contact (inset). The electronic circuit enables switching between conductance (red) and shot noise (blue) measurement modes.

For noise measurements, the sample is current biased and the voltage response is amplified by low-noise voltage amplifiers. The amplified voltage signal is recorded by a fast digitizer (NI 5992) and the power spectrum is calculated by digital Fourier transform. Two different configurations of voltage amplifiers were used for the experiments. In one configuration, an NF Li-75a was used, followed by a Signal Recovery 5184. The overall voltage amplification is 10^5 and the input voltage noise is 1.5 nV/$\sqrt{\text{Hz}}$. In a second configuration, a specially designed amplifier (JanasCard) with amplification of 10^4 and voltage noise of 0.9 nV/$\sqrt{\text{Hz}}$ is used. The lower voltage noise enabled a higher signal to noise ratio, which was important for shot noise measurements at high conductance values [$G = (5\text{–}15)G_0$]. The sample and amplifiers are located inside a specially designed Faraday cage in order to minimize noise pickup from environmental radiation. The piezo voltage is supplied by a differential voltage source and amplified by a factor of 4 using a Piezomechanik SVR-150 piezo driver.

B. Theoretical approach

In order to compute the conductance and shot noise of the atomic contacts studied experimentally, we have combined classical molecular dynamics (MD) simulations of the formation of the contacts, a tight-binding description of the electronic structure, and nonequilibrium Green's function techniques. Our methodology proceeds along the lines of Refs. [8,11,69,85–87]. In the following we briefly describe our approach.

Molecular dynamics simulations. In metallic atomic contacts there is a crucial interplay between mechanical and transport properties. Thus, in order to establish a direct comparison with our experiments, it is necessary to describe the formation process of these nanowires. For this purpose we have carried out MD simulations using the open source program package LAMMPS [88,89]. Within LAMMPS, we employed the embedded atom method with the semiempirical potentials from Ref. [90] for Ni and Cu, Ref. [91] for Co, and Ref. [92] for Fe to model the interactions between the atoms. These potentials take into account the possibility of having an atomic coordination different from bulk. To generate the geometrical configurations, we started with an ideal fcc lattice for Co, Ni, and Cu and an ideal bcc lattice for Fe where the crystal direction $\langle 100 \rangle$ lies parallel to the z axis, coinciding with the transport and elongation direction. For the simulations, we first divided the geometry into three parts: two electrodes and a central wire attached to them (see Fig. 2). The electrodes consist of 661 (321) atoms for fcc (bcc) each that are kept fixed during the MD calculations. The wire is made up of 563 (275) atoms that follow the Newtonian equations of motion. We assume a canonical ensemble and use the velocity Verlet integration scheme [93]. The simulated wires have an initial length of 0.57 nm for Fe, 0.75 nm for Co, and 0.73 nm for Ni and Cu. The starting velocities of the atoms in the wire were chosen randomly with a Gaussian distribution to yield an average temperature of $T = 4$ K. Because of this randomness, every elongation calculation evolves differently, while a Nosé-Hoover thermostat keeps the temperature fixed [93]. To relax the system, the wire gets equilibrated for 0.1 ns at the beginning of the elongation process. Finally, the elongation process is simulated by separating one electrode from the other at a constant velocity of 0.4 m/s. During this process, every 10 ps the geometry is recorded. A stretching process needs a total simulation time of about 5 ns, until the contact breaks.

Transport calculations. Once the geometries of the atomic wires are determined through the MD simulations, we use them to calculate the conductance and the shot noise within the Landauer-Büttiker formalism. Within this formalism all linear response transport properties are determined by the transmission function. To compute this function one needs, first of all, a proper description of the electronic structure of the metallic atomic contacts. For this purpose, we have employed the nonorthogonal Slater-Koster tight-binding parametrization of Refs. [94,95], which has been quite successful in determining a variety of properties of these atomic wires [8,11,69,85–87] and it is known to accurately reproduce the band structure and total energy of bulk ferromagnetic materials [96]. In this parametrization one takes into account the relevant valence orbitals of the material under study. For the four materials studied in this work (Fe, Co, Ni, and Cu), the atomic basis includes the $3d$,$4s$, and $4p$ orbitals. For the ferromagnetic materials, the on-site energies and hopping matrix elements depend on the electron spin and the model describes two independent sets of spin bands. In other words, there is no spin mixing in our model, as in the classical two-current model, which means in particular that we do not consider the spin-orbit interaction. This also means that we do not consider here the possibility of having magnetic domains in the atomic contacts. Within this tight-binding model, the hopping and overlap matrix elements are parametric functions of the distance between the atoms, which allows us to combine it with our MD simulations.

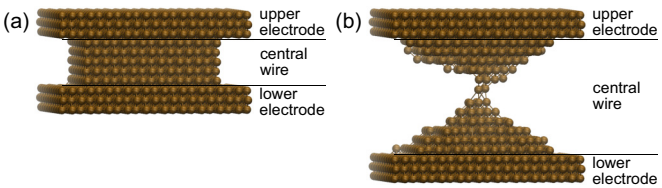

FIG. 2. Contact geometries in the molecular dynamics simulations. (a) Ideal fcc initial structure of the Ni contacts. (b) The same Ni contact as in panel (a) after an elongation of 1.4 nm. In both panels we have indicated the partitioning of the contact into the upper and lower electrodes and the central wire, as used for the MD and transport calculations.

We compute the transmission in the framework of our tight-binding model by making use of nonequilibrium Green's function techniques, as described in Refs. [69,85,86]. Briefly, as in the MD simulations, the system is divided into three regions for the transport calculations, i.e., the upper and lower electrodes and the central wire (see Fig. 2). As the local environment of the atoms in the central part is very different from that in the bulk, we enforce the charge neutrality for all the atoms of the wire [69]. Such a neutrality condition is typically a good approximation for metallic systems. The electrodes are considered to be semi-infinite perfect crystals. Their surface Green's functions are computed with the help of a decimation technique [69,97,98], and we use the same tight-binding parametrization as for the central part to determine their electronic structure. It is worth stressing that the Green's function techniques allow us to compute not only the transmission function, but also the spin-resolved transmission eigenvalues, $\{\tau_{n,\sigma}\}$, the analysis of which provides additional physical insight. Within the Landauer-Büttiker formalism the conductance G can be expressed in terms of $\{\tau_{n,\sigma}\}$ at the Fermi energy as [99]

$$G = \frac{G_0}{2} \sum_{n,\sigma} \tau_{n,\sigma}, \tag{1}$$

where $\sigma = \uparrow, \downarrow$ is the spin. At low temperatures and within the linear regime, the zero-frequency shot noise is given by $S_I = 2eIF$, where I is the bias current. The Fano factor F describes the noise suppression with respect to its full Poissonian value of $2eI$, and is given by

$$F = \frac{\sum_{n,\sigma} \tau_{n,\sigma}(1 - \tau_{n,\sigma})}{\sum_{n,\sigma} \tau_{n,\sigma}}. \tag{2}$$

To conclude this section, let us introduce the concept of minimum cross section (MCS), which provides a measure of

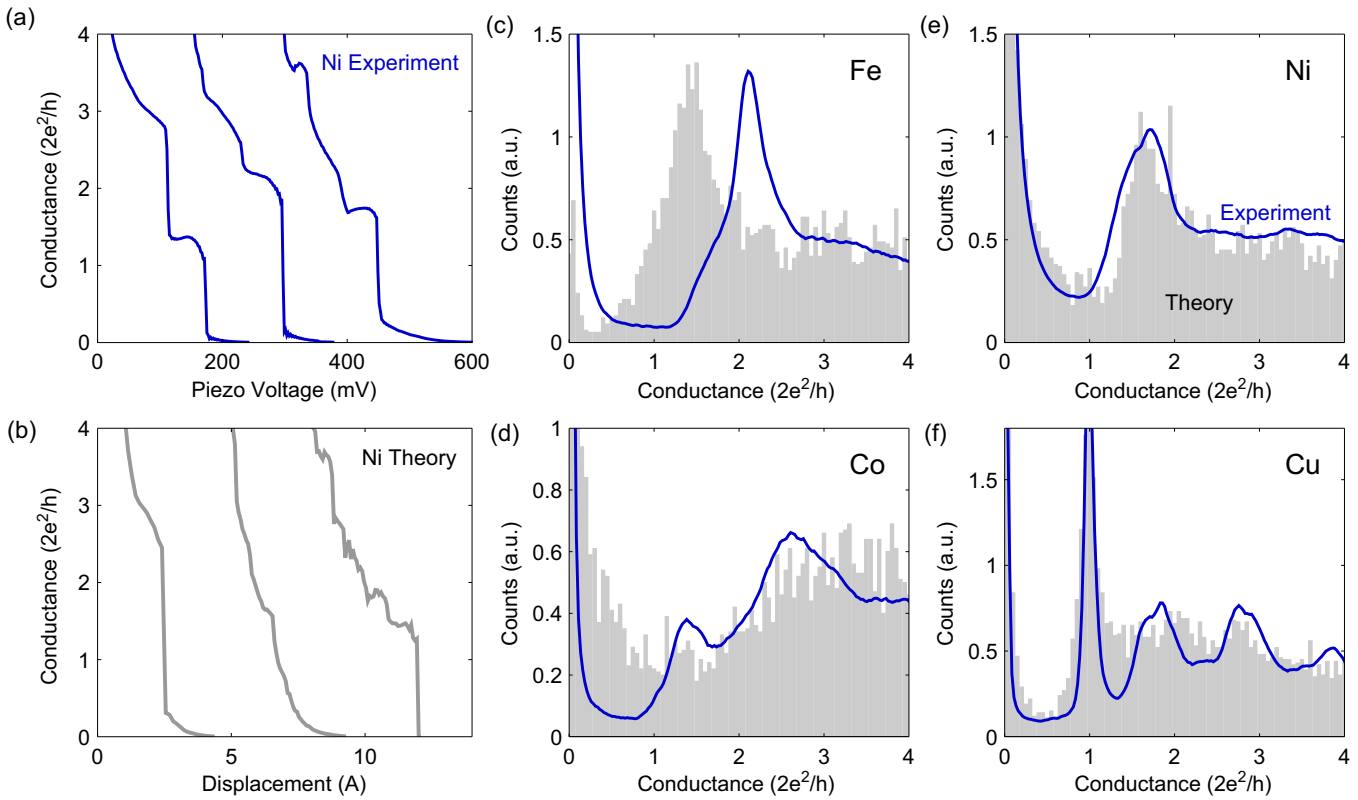

FIG. 3. (a) Ni conductance traces recorded in experiment at a bias of 50 mV. (b) Simulated Ni conductance traces. (c)–(f) Conductance histograms for Fe (c), Co (d), Ni (e), and Cu (f), constructed from experimental (blue line) traces, recorded at bias voltages of 50–150 mV, and simulated (gray area) traces. The experimental histograms were constructed from 10 000 traces for Co, Ni, and Cu and 5000 traces for Fe. The theoretical histograms include 100 traces each.

the contact size and the number of atoms in the narrowest part of the wire. As we shall see, this is a useful concept, but it must be acknowledged that there is no unambiguous way to define this quantity in an atomic-scale wire. In our simulations, we define and obtain this quantity as follows. We first superimpose our atomic structure with a fine-meshed grid with a grid spacing of about 0.02 nm. In analogy to a sandglass, we compute the total flow through the contact, which consists of the flows through all (one or more) bottlenecks connecting the two ends of the wire. Dividing the total flow by the possible flow through one atom, one gets the sum of the areas of all bottlenecks as function of atomic cross sections.

III. CONDUCTANCE HISTOGRAMS

To characterize the differences in transport and structural properties of Fe, Co, Ni, and Cu atomic contacts, we have measured their dc conductance (I/V) as a function of applied piezo voltage, during repeated breaking and reforming of the contact. Figure 3(a) shows examples of conductance traces recorded in the last stages of the breaking process of Ni contacts. As the minimal cross section of the contact is reduced, the conductance exhibits a sequence of plateaus separated by sudden jumps to lower conductance values. The plateaus correspond to relatively stable atomic configurations, which are separated by jumps due to sudden atomic rearrangements that occur once sufficient stress is accumulated [100]. Further elongation leads to rupture of the atomic contact and to a corresponding drop in the conductance. The small though nonvanishing measured conductance arises from electron tunneling between the broken atomic tips. Conductance traces obtained from our simulations of Ni contacts are presented in Fig. 3(b). As one can see, they nicely reproduce the slope of the conductance plateaus as well as the transition to the tunneling regime.

The observed variation from trace to trace stems from the different atomic geometries probed during each breaking cycle. To obtain a statistical picture of the typical conductance values characterizing each metal, we construct conductance histograms by collecting conductance values from thousands of experimental conductance traces. Figures 3(c)–3(f) show the conductance histograms obtained from experimental traces (blue lines). The histograms show different sets of peaks, which are interpreted as the conductance of frequently occurring atomic configurations [1]. For all ferromagnetic metals we find in common that the conductance peaks are located above the quantum of conductance (G_0) and that they exhibit a considerable width (FWHM $\sim 1G_0$). These observations are in good agreement with previously reported measurements in inert environments by Untiedt *et al.* [40]. In contrast, in the case of the monovalent metal Cu, the conductance histogram [Fig. 3(f)] exhibits a series of relatively narrow peaks close to multiples of G_0. Our results therefore indicate the absence of any kind of conductance quantization (either integer or half integer) for ferromagnetic contacts.

For comparison with the experimental data, we have computed conductance histograms from 100 breaking simulations

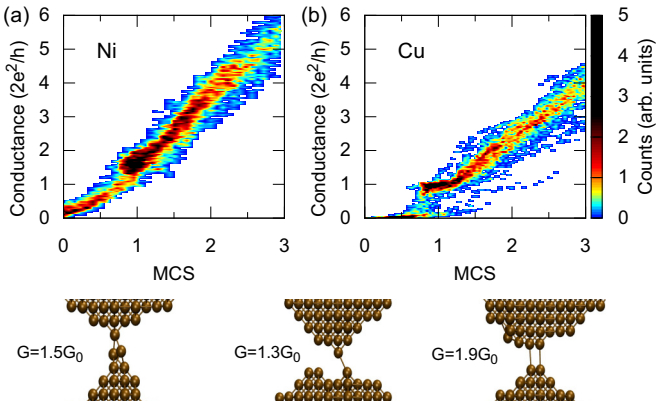

FIG. 4. Density plots of conductance vs minimal cross section (MCS) for Ni (a) and Cu (b) obtained from 100 simulated traces. Lower panels: Examples of simulated configurations of Ni atomic contacts that contribute to the main peak in the conductance histogram; see Fig. 3(e). The calculated conductance is indicated next to each contact.

for every metal [gray areas in Figs. 3(c)–3(f)]. As one can see, there is generally a good agreement between theory and experiment in the locations and widths of the peak features for the different metals. One exception is the observed shift in the peak position of the simulated Fe histogram with respect to experiment. A possible explanation for this difference could be that the Fe potential, created for the crystalline phase with defects and for the liquid phase, is not able to provide a good enough description of the low-coordinated environment near the ending of the rupture process, despite its advantages from the embedded atom method (EAM) formalization. We tried different EAM potentials and different elongation directions, but the agreement with the experimental data did not improve significantly. Nevertheless, the reproduction of most of the experimental features indicates that our simulations provide a good description of the structural and transport properties of the examined atomic contacts. This is reinforced by the good agreement found for the shot noise results, as we shall discuss in the next section.

To understand the features observed in the conductance histograms, we turn to the analysis of the relation between conductance and structure in the simulated atomic contacts. An important structural parameter that is correlated with the transport properties is the minimal cross section (MCS) of the contact, whose precise definition was provided at the end of Sec. II B. Figures 4(a) and 4(b) show 2D density plots of the MCS and conductance obtained from the contact geometries probed in our simulations for Ni and Cu. From these figures, we can see that the conductance of the last peak can be mainly ascribed to a contact with a single-atom constriction. For Ni, the conductance of the last peak [$\sim(1.2–2.2)G_0$] corresponds to a MCS of 0.7–1.3, while for Cu the conductance range [$\sim(0.8–1.2)G_0$] corresponds approximately to MCS values of 0.7–1.3. We have obtained similar conclusions for Fe and Co contacts.

For all ferromagnetic contacts we find a large variance in the conductance for a given MCS value as compared with Cu. This observation indicates that the conductance of ferromagnetic contacts is more sensitive to the exact atomic configuration than in noble metals. Moreover, notice that for a given value of the MCS, the conductance of Ni contacts (and also Fe and Co contacts, not shown here) is higher than that of Cu contacts, which is clearly at variance with what happens in macroscopic wires of these materials.

The lower panels of Fig. 4 show three typical configurations of Ni contacts exhibiting conductance values in the range of the main conductance peak. We find two types of configurations which can be defined as single-atom contacts: a single atom bonded to two or more atoms on each side (left contact) and contacts that show two undercoordinated atoms with a single bond on one side (central contact), which we will refer to as monomer and dimer, respectively. Note that configurations that cannot be defined as a single-atom contact (see right contact) also contribute to the conductance peak. In any case, the fact that these three different geometries contribute to the Ni conductance peak shows that it is not straightforward to establish a one-to-one correspondence between conductance peaks and atomic structures, especially in the case of multivalent metals. A similar variability is also found in the atomic configurations corresponding to the peaks in Fe and Co. In the case of Co, for which two peaks are observed, we find that the examined configurations contributing to the lower conductance peak can be mainly identified as single-atom contacts (i.e., monomer and dimer configurations), while also other configurations can contribute to the higher conductance peak.

Interestingly, Figs. 4(a) and 4(b) show a clear linear relation between the conductance and MCS, reflecting the dependence expected from Sharvin's conductance formula for a ballistic constriction [101]. The observation that the linear relation extends almost all the way down to the single-atom level may seem quite surprising since, as we have seen above, the conductance is highly sensitive to small changes in the atomic geometry. The results of Figs. 4(a) and 4(b) also show that there is a considerable variance of the conductance for a given MCS value. Thus for instance, the conductance for a Ni contact with a MCS of 1 atom can vary between $1G_0$ and $2G_0$. Therefore, the scaling of the MCS should be understood for the average conductance of many contact geometries.

IV. SHOT NOISE

To further investigate the transport properties of ferromagnetic contacts, we have conducted measurements of the electronic shot noise generated by the contacts. Let us remind the reader that within the Landauer-Büttiker framework, shot noise depends on the number of open conduction channels and their transmission probabilities; see Sec. II B. The overall zero-frequency current noise generated by a quantum conductor (including the thermal noise) can be expressed as [6,102]

$$S_I = 4k_B T G[1 + F(x\coth(x) - 1)], \tag{3}$$

where G and F are the conductance and Fano factor, respectively [see Eqs. (1) and (2)], and $x = eV/2k_BT$ describes the ratio between bias voltage V and temperature T. Near equilibrium conditions ($x \ll 1$), S_I reduces to the Johnson-Nyquist expression for thermal noise $4k_BTG$. At high bias ($x \gg 1$), the current noise depends linearly on the bias current, $S_I = 2eIF$. Figure 5 shows an example shot noise

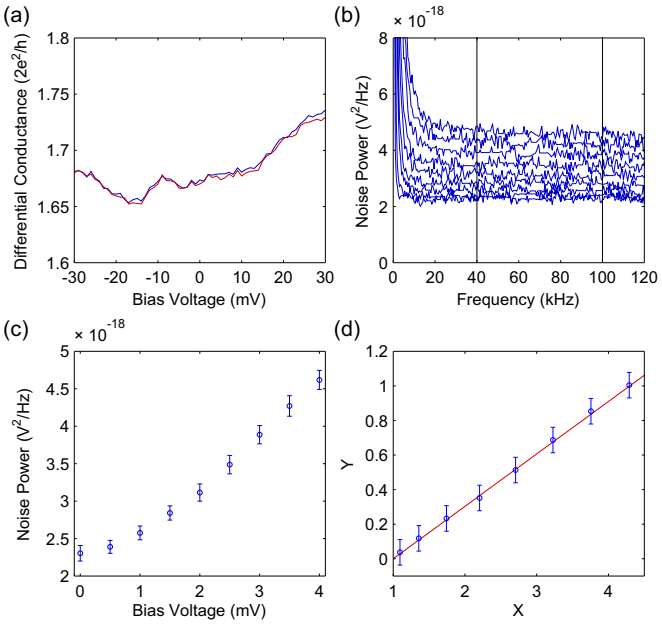

FIG. 5. (a) Differential conductance (dI/dV) curve measured for a Ni atomic contact before (blue) and after (red) shot noise measurements. (b) A series of noise spectra recorded at different bias voltages. Black lines indicate the frequency window which was selected for obtaining the average noise power. (c) Average noise power as function of bias voltage. (d) Dependence of the reduced values X,Y (blue) calculated for the measured noise in (c), and a linear fit (red), giving $F = 0.30 \pm 0.01$ according to Eq. (4).

measurement for a Ni atomic contact. Differential conductance spectra (dI/dV) of the contact, see Fig. 5(a), are recorded before and after the noise measurement in order to confirm that the junction has remained stable during the measurement. The zero-bias conductance of the junction is determined from the average differential conductance in the window of $|V| < 5$ mV. Figure 5(b) shows a series of noise spectra for different applied bias. Each spectrum is obtained from the Fourier transform of voltage fluctuations produced by the junction, and averaged for 5000 consecutive measurements. The voltage noise produced by the amplifier was measured separately and subtracted from the recorded spectra. The spectra were corrected to account for low-pass filtering due to capacitance of the cabling and amplifier input capacitance (total capacitance of ∼40 pF). The noise power is averaged in a frequency window, which is selected to be high enough to reduce $1/f$ noise contributions. Figure 5(c) shows the average noise power as a function of bias voltage across the junction. Following Ref. [6], Eq. (3) can be expressed as

$$Y = F(X - 1), \tag{4}$$

where $X = x\coth(x)$ and $Y = [S_I(V) - S_I(0)]/S_I(0)$. The Fano factor is obtained by calculating the reduced parameters X,Y and obtaining a linear fit of $Y(X)$ according to Eq. (4), as shown in Fig. 5(d). Occasionally, we observed zero-bias anomalies in the differential conductance curves that may originate from different possible mechanisms, including Kondo physics [47,81]. In all the studied cases the magnitude of the observed features was limited to several percent of the total conductance, while the related shot noise could be described very well by Eq. (3), in the framework of Landauer formalism. Both these observations indicate that the physical mechanism related to the zero-bias anomalies has a relatively small effect on the distribution of conduction channels of the atomic contacts studied here.

Figure 6 shows the distribution of F as function of zero-bias conductance G obtained for Fe, Co, Ni, and Cu atomic contacts. For Cu, a suppression of the Fano factor towards its lower limit for spin-degenerate transmission (light shaded area) is observed. This behavior is similar to the results obtained for the monovalent metals Au and Ag, indicating conductance quantization, i.e., that in multiples of G_0 the conductance takes place through nearly fully open channels [3,7]. Conversely, a distinct qualitative picture arises for ferromagnetic contacts. The measured values of F are found to be significantly higher compared to Cu. In particular, the large suppression at multiples of G_0 observed for Cu is clearly missing for the ferromagnetic contacts.

The conductance and Fano factor depend on the distribution of conduction channels carrying the current, in accordance with Eqs. (1) and (2). This dependency allows us to draw several conclusions regarding the set of transmission probabilities $\{\tau_{n\sigma}\}$. First, one can determine the minimum number of channels contributing to transport according to the position of the measurement in the (F,G) space. The solid lines starting from $(F,G) = (1,0)$ and ending at $(0,Ne^2/h)$ in Figs. 6(a)–6(c) indicate the maximum Fano factor that can be obtained for N spin channels (i.e., having a maximum conductance of Ne^2/h). Therefore, given a combination of (F,G) one can obtain a lower bound for the number of transmitting channels [indicated within the regions between each two lines in Fig. 6(c)]. For Ni, one can see that a minimum of $N = 3$–6 spin channels contribute to transport for contacts with conductance values corresponding to configurations with single-atom cross section [i.e., ∼(1.2–2.2)G_0; see Fig. 3(e)]. Similarly, the results for Co and Fe indicate that the current through a single-atom contact is carried through a multiple number of channels.

To study the transmission values $\{\tau_{n\sigma}\}$, we use a numerical analysis introduced in Ref. [7]. The analysis is based on enumerating the possible combinations of $\{\tau_{n\sigma}\}$ up to a certain number of channels N (here, $N = 6$ was chosen to account for the main channels), and identifying the range of solutions that give the measured F and G. In many cases, this analysis allows us to determine the transmission probabilities with reasonable accuracy. We note that since Eqs. (1) and (2) are symmetric with respect to spin, the spin direction cannot be determined using this method. The transmission probabilities are labeled by a single index i, and are ordered according to decreasing transmission. Figure 6(d) shows the possible values of $\{\tau_{n\sigma}\}$ for three different combinations of F and G for Ni contacts, which are indicated in Fig. 6(c). For combination 1 (bottom panel), in which the Fano factor is near its minimum limit, two fully open spin channels carry most of the current. In the case of Cu, for which spin polarization is not expected, measurements located at this position indicate transport dominated by two channels (one for each spin type) with identical transmission. As can be seen from examples 2 and 3 [middle and upper panels in Fig. 6(d)], an increase in F results in a larger number of partly

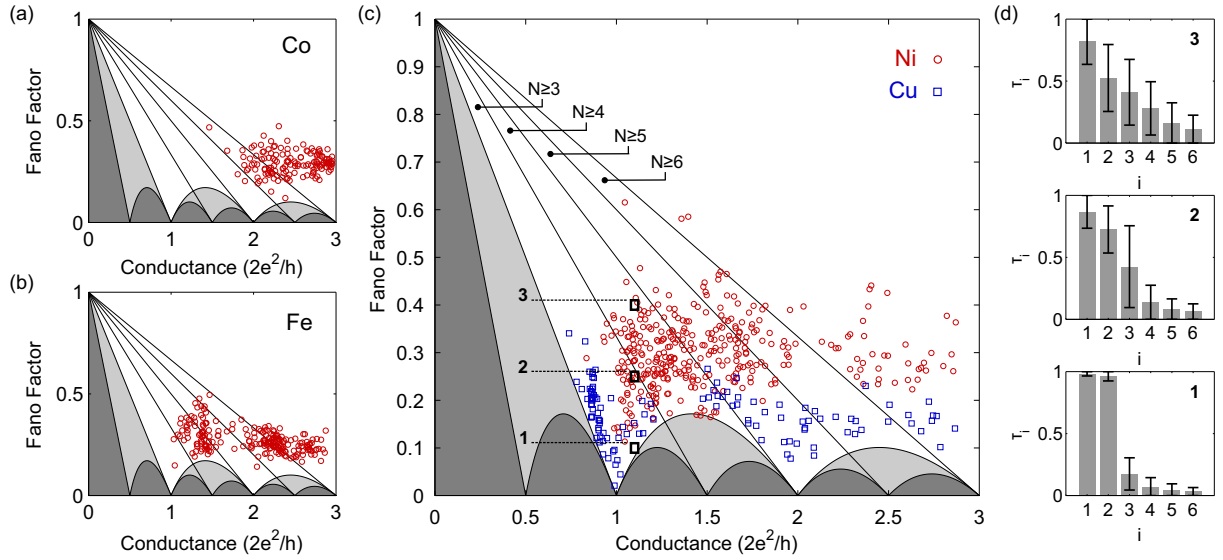

FIG. 6. (a)–(c) Fano factor as a function of the conductance as obtained from shot noise measurements for Co (a), Fe (b), Ni [(c), red circles], and Cu [(c), blue squares]. Shaded areas show the inaccessible regions for the case of spin-degenerate transport (light shaded) and for the general case (dark shaded). Black lines starting from $(F,G) = (1,0)$ and ending at $(0, Ne^2/h)$ indicate the maximum F obtainable for N spin channels (see text). The measurement errors $\Delta G, \Delta F$ do not exceed $0.02G_0$ and 0.03, respectively, for Cu and Ni, and $0.04G_0$ and 0.04 for Fe and Co. (d) Spin-dependent conduction channel distributions for Ni contacts with measured values of $G = 2.2 \pm 0.04e^2/h, F = 0.40 \pm 0.01$ (top panel), $F = 0.25 \pm 0.01$ (middle), $F = 0.10 \pm 0.01$ (bottom). These values of conductance and Fano factor are indicated as black squares in (c). Error bars indicate minimum and maximum possible transmission for each spin channel.

open channels carrying the current. This trend appears for any conductance range; a low Fano factor near the minimum limit indicates a channel distribution with a minimal number of channels and a maximal number of open channels ($\tau_{n\sigma} = 1$), while a higher F results in a distribution with a larger number of channels and lower transmission values. Thus, the large spread in F observed for Fe, Co, and Ni implies that there is no conductance quantization, while the number of channels and their transmission probabilities vary significantly between different contact realizations.

Our analysis of conductance traces and shot noise measurements indicates that the conductance and channel distribution in ferromagnetic contacts are highly sensitive to atomic geometry. This sensitivity makes the comparison between theory and experiment challenging. Interestingly, the structure-conductance analysis obtained from our simulations (Fig. 4) shows that the relative variance of the conductance in respect to the mean value ($\Delta G/G$) is greatly reduced with increasing MCS. Thus, the study of larger contacts could be advantageous as the sensitivity to atomic geometry is significantly reduced. Unfortunately, the conductance histograms for ferromagnetic contacts do not show clear features at values above $\sim 4G_0$. On the other hand, the study of shot noise at larger conductance values could potentially provide new information, allowing a more straightforward comparison with theory.

To investigate this possibility, we have extended our measurements and simulations to contacts with higher conductance values, focusing on Ni and Cu for comparison between a ferromagnetic metal and a monovalent metal. Figure 7(a) shows the distribution of the Fano factor as function of conductance measured up to $15G_0$, for Ni and Cu contacts. Remarkably, for both metals, the variance in the Fano factor

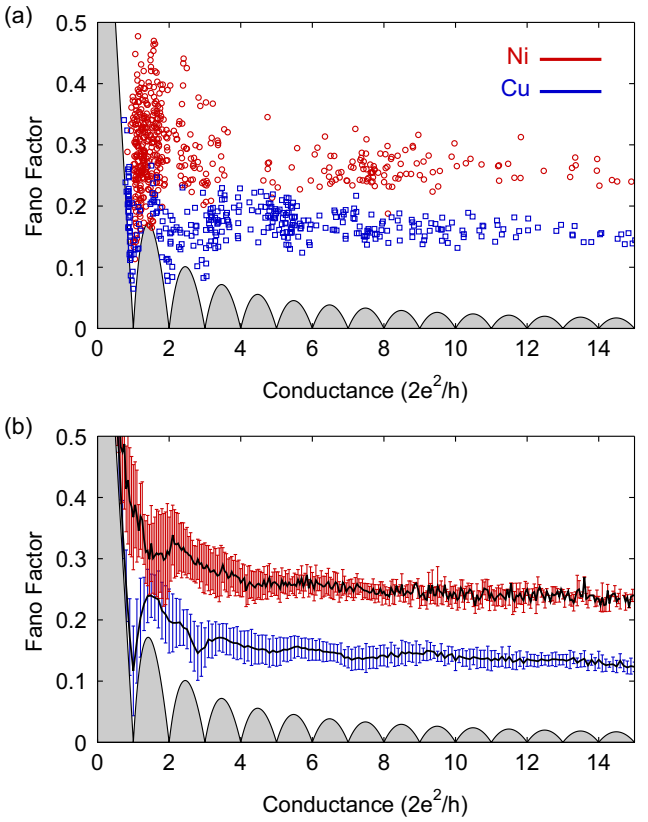

FIG. 7. Saturation of Fano factor. (a) Measured Fano factor as a function of the conductance for Ni contacts (red) and Cu contacts (blue). (b) The corresponding computed Fano factor as a function of conductance. The solid lines indicate the average value, while error bars show the corresponding standard deviation.

is strongly reduced for larger contacts, and the Fano factor saturates to a nearly constant value of 0.26 ± 0.02 and 0.15 ± 0.01 for Ni and Cu, respectively.

Figure 7(b) shows the (F,G) distribution obtained from our simulations. The results are found to be in very good agreement with the experimental values, both in the large variance at low conductance and in the saturation at higher conductance values. The simulated saturation values obtained yield 0.23 ± 0.01 and 0.13 ± 0.01 for Ni and Cu, respectively. Our simulations for Fe and Co result in similar behavior to that obtained for Ni, both giving the same saturation value of 0.27 ± 0.01; see the Appendix. For Au, having a monovalent orbital structure similar to Cu, the Fano factor obtained by our simulation reaches a value of 0.15 ± 0.02. We note that previous measurements for Au contacts have indicated an average F of $\sim$0.15 for $G > 10G_0$ [103]. Thus, the clearly larger Fano factor values encountered in the ferromagnetic metals as compared to the noble ones seem to be a generic feature, which reflects the different orbital structure of these two kinds of metals. This observation will be further discussed in the following section.

V. NATURE OF THE CONDUCTION CHANNELS

The goal of this section is to elucidate the transport mechanism in ferromagnetic atomic contacts by analyzing the electronic structure and conduction channels of our simulated atomic contacts. We shall show that the fundamental differences between noble and ferromagnetic metals are related to the significant role that d orbitals play in the transport properties in the latter case. Furthermore, we find that the exchange splitting of the d orbitals results in distinct transport for majority-spin and minority-spin electrons. For didactic reasons, in this section we focus on the comparison between Ni and Cu. We find that the conclusions drawn for Ni are qualitatively valid for Fe and Co. Our theoretical results for these metals are shown in the Appendix.

Figure 8 shows a comparison of the energy dependence of both the density of states (DOS) and the transmission function for Ni and Cu, as calculated from our tight-binding model. The upper panels show the bulk DOS, while the middle panels display the local DOS projected onto the central atom for a single-atom contact configuration. The contributions of $3d$,$4s$, and $4p$ orbitals to the DOS are shown in separate curves. In the case of Ni, we show separately the contributions of the majority-spin (or spin-up) electrons and minority-spin (or spin-down) electrons to both DOS and transmission. Comparing these figures, one can immediately see that the main difference between Ni and Cu is the large contribution of d orbitals at the Fermi energy for Ni. This contribution is particularly large in the case of minority-spin electrons, for which the d states are located higher in energy due to the spin splitting for the bulk d bands.

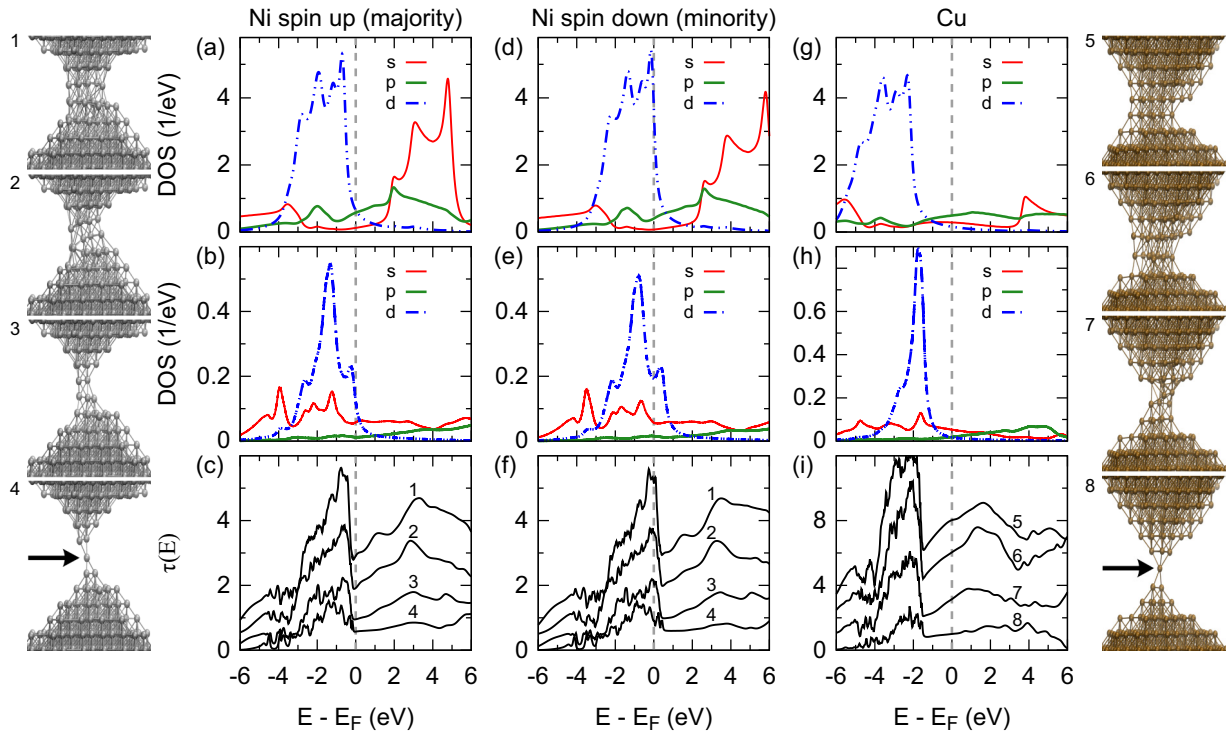

FIG. 8. (a) Bulk density of states (DOS) as a function of energy for the majority-spin (or spin-up) bands of Ni. We show the total contribution of the $3d$,$4s$, and $4p$ orbitals normalized by the number of orbitals in each of these groups. (b) The energy dependence of the local DOS for majority spins projected onto the central atom (see arrow) of the Ni single-atom contact number 4 shown in the left column. Again, the different curves correspond to the normalized total contributions of the s, p, and d orbitals. (c) The total transmission as a function of energy for the majority spins for the four Ni contacts shown in the left column which were obtained in one of the simulations of the breaking process. (d)–(f) The same as in panels (a)–(c) for the minority-spin electrons. (g)–(i) The same as in panels (a)–(c) for Cu. The corresponding Cu contact geometries are shown in the right column. In all panels, the vertical dashed lines indicate the position of the Fermi energy, as a guide to the eyes.

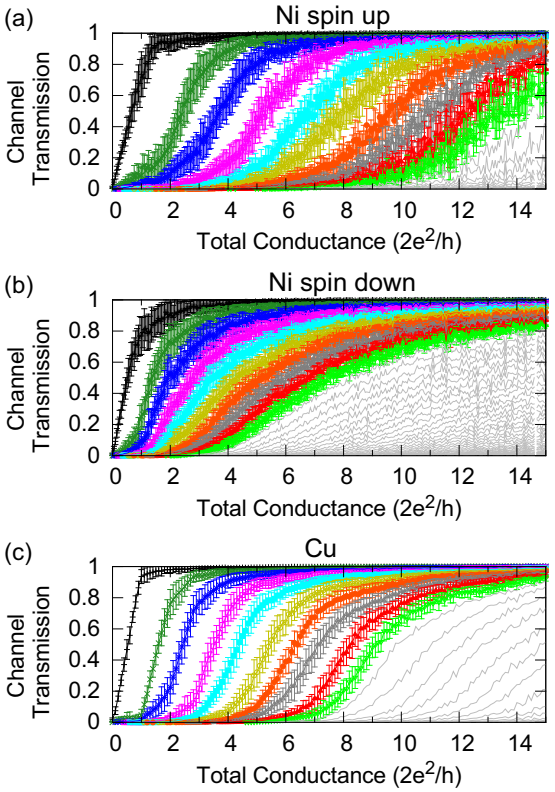

FIG. 9. (a) Transmission coefficients for Ni majority-spin (spin-up) electrons as a function of the contact conductance. The lines indicate the average values and the bars the standard deviations. (b) The same as in panel (a) but for Ni minority-spin (spin-down) electrons. (c) The corresponding results for Cu.

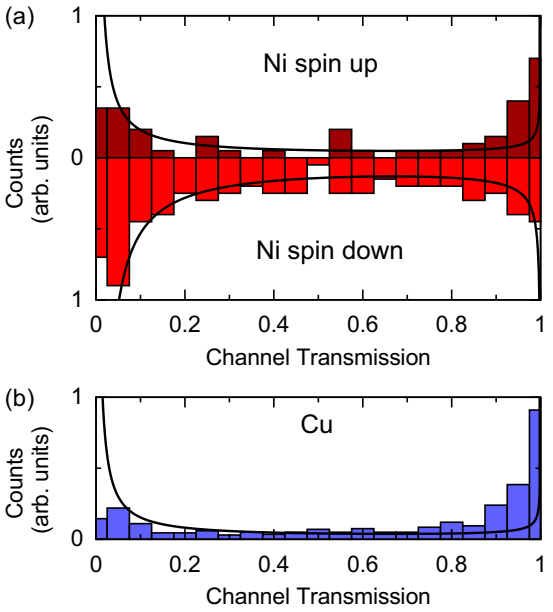

FIG. 10. (a) Transmission coefficient histogram for Ni contacts with a conductance of $15G_0$. We show the results for both majority-spin (spin-up) electrons and minority-spin (spin-down) electrons. (b) The corresponding results for a Cu with $G = 15G_0$. In both panels the solid lines show the bimodal distribution of Eq. (5).

The lower panels of Fig. 8 show the total transmission as a function of energy for four different contacts with different cross sections obtained in an individual simulation of the breaking process of a Ni and a Cu wire. The corresponding contact geometries are shown in the left (Ni) and right (Cu) columns. As one can see in Figs. 8(c) and 8(f), the corresponding spin-resolved total transmission follows closely the energy dependence of the total DOS. Thus for instance, the total transmission at the Fermi energy, $\tau(E_F)$, for the minority-spin electrons is significantly higher than that of the majority-spin electrons, in correlation with the higher DOS at E_F in the former case. These results strongly suggest that d orbitals are responsible for the significantly higher transmission for minority-spin electrons. Importantly, we find that the key role of the d orbitals in transport properties also extends to atomic contacts with larger contact sizes.

To further study the transport mechanism in ferromagnetic contacts, we examine the distribution of conduction channels. Figure 9 shows the average value of the transmission probabilities as a function of conductance as obtained from 100 contact stretching simulations for Ni (spin up and down) and Cu. In the case of Ni, one can immediately see that there is a larger number of channels contributing to transport for minority-spin electrons. For example, for conductance values related to a single-atom Ni contact [i.e., $\sim(1.2–2.2)G_0$], there are approximately 4–7 minority-spin channels compared to 2–4 majority-spin channels. The larger number of minority-spin channels can be correlated with the higher number of the minority-spin d states at E_F [Figs. 8(d) and 8(e)], which are available for conduction electrons.

In the case of Cu [Fig. 9(c)], we see that transport is dominated by channels with nearly perfect transparency which open one by one with increasing conductance. This behavior naturally explains the suppression of shot noise at multiples of G_0 observed for this metal. As the conductance increases (or equivalently the contact size) more partially open channels appear, explaining why the Fano factor does not vanish for contacts with conductance above $3G_0$. Interestingly, a tendency for transport through nearly open channels is also observed for Ni spin-up electrons [Fig. 9(a)]. However, as the transport is mainly carried by spin-down channels with intermediate transmission values, one does not observe any strong suppression of the Fano factor at any particular value of the conductance.

To understand the origin of the saturation of the Fano factor and the differences in the saturation values between Cu and the ferromagnetic metals, we show in Fig. 10 histograms of the transmission eigenvalues for Ni and Cu contacts with a conductance of $15G_0$. As one can see in Fig. 10(a), the spin-up and spin-down transmission coefficients are distributed very differently. In the former case, the distribution shows a preference to open channels. In contrast, for minority spins, the distribution is mainly composed by partially open channels. As discussed in Sec. IV, the Fano factor increases as the conductance is determined by a larger number of partially open channels. Thus, from the transmission histograms, we can conclude that the lower value of the Fano factor at saturation in the case of Cu results from the dominant role of nearly fully

open channels, while for Ni this value is significantly larger due to the presence of numerous partially open (minority-spin) channels.

The results presented so far indicate that transport for Ni spin-up and spin-down electrons differs not only in the total transmission value, but exhibits fundamentally distinct behaviors. The transmission distribution for the majority spins clearly resembles that of the Cu contacts [Fig. 10(b)], in which transport is dominated by highly transmissive channels. This behavior can be traced back to the fact that in both cases (Cu and Ni spin-up), the states available for transport originate mainly from the s valence orbitals. On the other hand, the channel distribution of the Ni minority spins is very similar to that of the transition metal Pt [11], with dominant d valence orbitals near the Fermi energy. Thus, we see that Ni behaves in some sense as a combination of monovalent and transition metal conductors in parallel.

As it is well known in mesoscopic physics, the Fano factor of a metallic diffusive wire is universal (it does not depend on the degree of disorder or on the wire geometry) and adopts a value equal to 1/3 [104,105]. This value can be understood in terms of the distribution of transmission coefficients, which in the diffusive wire case reduces to the so-called bimodal distribution [106,107]

$$P(\tau) = \frac{G}{G_0}\frac{1}{2\tau\sqrt{1-\tau}}, \tag{5}$$

where $P(\tau)$ is the probability density to find a given value of the transmission τ and G is the wire conductance. To understand the differences between our atomic contacts and the diffusive wire case, we show in the histograms of Fig. 10 the bimodal distribution of Eq. (5) as a solid line. As one can see in Fig. 10(a), the distribution of the Ni minority spins follows the bimodal distribution. Indeed, the Fano factor for the minority-spin electrons $F_\downarrow = \sum \tau_{n,\downarrow}(1-\tau_{n,\downarrow})/\sum \tau_{n,\downarrow}$ yields 0.28, 0.30, and 0.34 for Ni, Co, and Fe, respectively. These values are very close to the universal value of 1/3. Thus, our results suggest that ferromagnetic atomic contacts show a diffusive-like behavior for minority-spin electrons. On the other hand, the transmission distributions for the Ni majority spins and for Cu differ markedly from the bimodal distribution, the main difference being the presence of a larger number of channels with very high transmissions. This fact leads to a reduction of the Fano factor as compared to the diffusive case. In this respect, we find that the Fano factor for the Ni majority-spin electrons is $F_\uparrow = 0.16$, while $F_\uparrow = 0.22$ for Co and $F_\uparrow = 0.20$ for Fe. These values are closer to the saturation value for Cu, $F = 0.15$. We will further discuss these results in the following section.

Another aspect of the conduction across ferromagnetic atomic contacts that differs dramatically from the macroscopic case is the spin polarization of the current. This quantity is defined as

$$P_I = \frac{I_\uparrow - I_\downarrow}{I_\uparrow + I_\downarrow} \times 100\%, \tag{6}$$

where $I_\uparrow$ is the current carried by the majority-spin electrons and $I_\downarrow$ is the current carried by the minority-spin electrons. In the case of macroscopic wires, Mott's model predicts a positive sign for the spin polarization because transport is dominated by majority-spin electrons, as explained in the introduction. The positive spin polarization was found to be consistent with studies of subgap-structure measurements of ferromagnet-superconductor interfaces [108]. In contrast, following our discussion above, it is clear that in the case of atomic-size contacts, the current is dominated by minority-spin electrons. The influence of this property is illustrated in Fig. 11, showing the current spin polarization as a function of the conductance. As one can see, the spin polarization is negative, irrespective of the conductance value, and it saturates to a value of $\sim -30\%$ for large contacts. Interestingly, while the presence of spin-down d states at the Fermi energy reduces the minority-spin conductivity in the bulk case, for atomic contacts the situation is precisely the opposite: additional minority-spin channels with d character become available for transport, resulting in an opposite sign of the spin polarization.

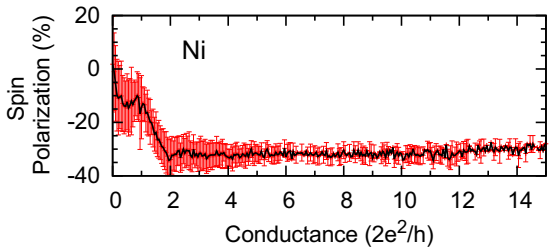

FIG. 11. Computed spin polarization of the current as a function of the conductance for Ni. The solid lines correspond to the average value and the bars to the standard deviation.

VI. DISCUSSION

Our results from both experiment and theory clearly indicate that d orbitals are responsible for fundamental differences in transport properties of ferromagnetic contacts compared to monovalent contacts. Ferromagnetic contacts clearly differ from Cu (and other monovalent metals) by (i) higher conductance, (ii) larger variance in the conductance and shot noise (for small contacts), (iii) existence of multiple partly transmitting channels, and (iv) nearly double Fano factor saturation value for large contacts. As our channel analysis reveals, transport in ferromagnetic contacts can be viewed to occur in parallel through spin-up channels, behaving similarly to a monovalent metal, and spin-down channels, acting as a transition metal. Thus, the aforementioned properties can be mainly attributed to the contribution of minority-spin electrons, for which d states are available for transport.

We will therefore divide our discussion into s-dominated transport (e.g., Cu, Ni spin-up) and transport through mixed sd states (e.g., Ni spin-down). In the case of s-dominated transport, conductance quantization, i.e., transport through fully open channels, takes place only for small contacts ($G \lesssim 3G_0$), whereas for larger contacts, an increasing contribution of partially open channels is observed. This behavior was reasonably reproduced by a model of a free-electron constriction with disorder, connecting two gradually narrowing contacts [109,110]. The mentioned disorder can be associated with local impurities, scattering at the contact surfaces or lack of periodical lattice structure. Indeed, one could naturally

expect that as the constriction size increases, the series resistance induced by disorder will play a more dominant role in transport, obscuring the measurement of quantized values of conductance. We argue that the saturation of the Fano factor could be viewed as an interplay between the quantization of the contact on one hand and some amount of disorder which results in imperfect transmissions. These arguments explain why the average value of the Fano factor ($\sim$0.15) is significantly lower than the value of $1/3$ expected for a diffusive contact.

In the case of transport with *sd* character, our results suggest that disorder is significantly higher compared to a monovalent conductor. We find this expressed in the bimodal distribution observed for spin-down Ni channels (and the corresponding $F_{\downarrow} \sim 1/3$), being a characteristic of diffusive transport. A higher disorder in ferromagnetic contacts can be related to the inherent anisotropy of *d* orbitals compared to the high symmetry of *s* orbitals. The interplay between the disorder in diffusive wires and a ballistic quantum point contact has been studied theoretically by Beennakker and Melsen [111]. The model analyzed in that work was able to recover the saturation of the Fano factor to $1/3$ with increasing contact size; however the channel distribution obtained for narrow contacts is at variance with the partially open channel distribution we obtain. This discrepancy indicates the need to consider the specific orbital structure of the contacts.

We note that Riquelme *et al.* [112] reported an experimental analysis of the transmission distribution of Pb atomic contacts with conductance values ranging between $1G_0$ and $15G_0$. The study was based on the use of superconductivity and the analysis of the subgap current, in the spirit of Refs. [2,83]. The authors concluded that as the contact size increased, the transmission distribution approached very quickly the universal bimodal distribution. Those authors also presented a theoretical analysis based on ideal geometries and a tight-binding model similar to the one employed here that suggested that this behavior could be associated with the *sp* valence orbital structure of Pb that gives rise to a significant contribution of partially open channels even in the absence of atomic disorder. This conclusion, together with our results, suggests that such behavior may be a general characteristic of multivalent metals.

When discussing diffusive transport in atomic contacts, it is important to consider the conductor dimensions. The strict definition of diffusive transport requires that the length of the conductor satisfies $L \gg \ell$, where ℓ is the elastic mean-free path. In the case of atomic contacts made of the monovalent metal Au, different estimates of ℓ give a value of approximately 4–5 nm [9,31,113]. In comparison, the length of the contacts in our simulations is up to 3 nm in total. Since the saturation of the Fano factor is captured in our simulated structures, we infer that this region is sufficient to describe the main transport characteristics. Thus, it is rather unlikely that the condition $L \gg \ell$ for diffusive transport is met. Yet, we can find two reasons why diffusive behavior is seen nevertheless.

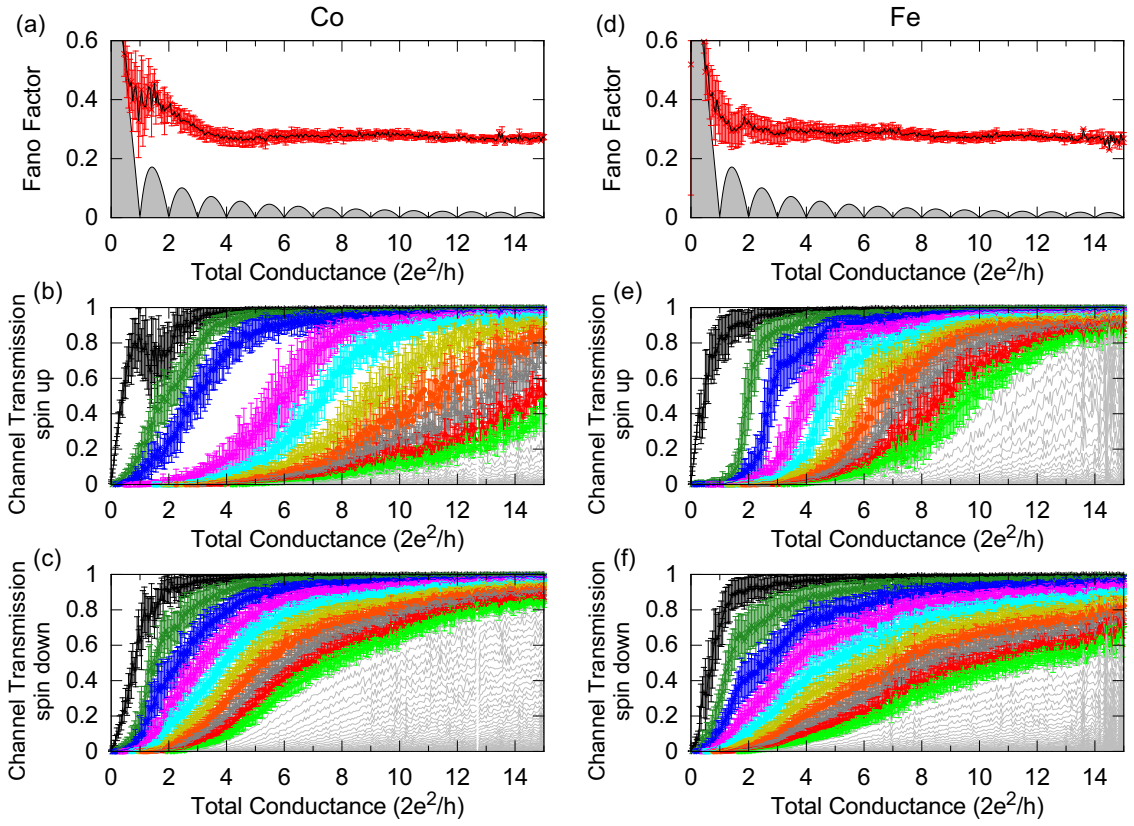

FIG. 12. (a) Computed Fano factor as a function of the conductance for Co contacts. The solid (black) line corresponds to the average value, while the (red) bars show the standard deviation. (b), (c) The spin-resolved transmission coefficients for Co majority-spin (spin-up) electrons (b) and for Co minority-spin (spin-down) electrons as a function of the contact conductance. The lines indicate the average values and the bars the standard deviations. (d)–(f) The same as in panels (a)–(c) but for Fe contacts.

First, the increased disorder originating from the contribution of d orbitals could lead to a considerably lower value for ℓ compared to Au. Second, theoretical studies have shown that it is sufficient to have a small number of tunneling barriers in series to result in a Fano factor near 1/3 [114]. These considerations can explain why the bimodal channel distribution can appear even in contacts of several atoms in cross section.

VII. SUMMARY

To summarize, we have presented a comprehensive experimental and theoretical study of the conductance and shot noise in ferromagnetic atomic contacts made of Ni, Co, and Fe, and we have compared the results with those for the nobel metal Cu. Our experimental results reveal clear differences between the ferromagnetic contacts and those made of Cu such as the absence of any type of conductance quantization and the larger values of the Fano factor for any conductance value (including the saturation value for large contacts) in the ferromagnetic case. Our theoretical results, which are able to satisfactorily reproduce our main experimental observations, clearly show that the transport properties of the ferromagnetic contacts can be explained in the framework of quantum coherent transport.

Our results demonstrate that the d orbitals (especially those of the minority-spin electrons) play a fundamental role in the transport through ferromagnetic atomic contacts. The contribution of these d orbitals leads to the appearance of partially open channels, which explains the absence of conductance quantization and the large values of the Fano factor, as compared to noble metals. Moreover, the contribution of minority-spin channels makes the ferromagnetic contacts more conductive than the noble metallic contacts and leads to negative values of the spin polarization, both observations in stark contrast with the behavior of macroscopic metallic wires. Thus this work provides a textbook example of how the transport properties of metallic wires can drastically change upon shrinking their characteristic dimensions to the atomic scale, a change that is due to modification in the dominant transport mechanism.

ACKNOWLEDGMENTS

The authors thank A. Halbritter for fruitful discussions. M.M. and P.N. acknowledge financial support from the SFB767 and computer time granting from the NIC and the bwHPC framework program of the State of Baden-Württemberg. J.C.C. acknowledges financial support from the Spanish Ministry of Economy and Competitiveness (Contract No.FIS2014-53488-P). O.T. thanks the Harold Perlman family for their support and acknowledges funding by the Israel Science Foundation (Grant No.1089/15) and the Minerva Foundation (Grant No.711136).

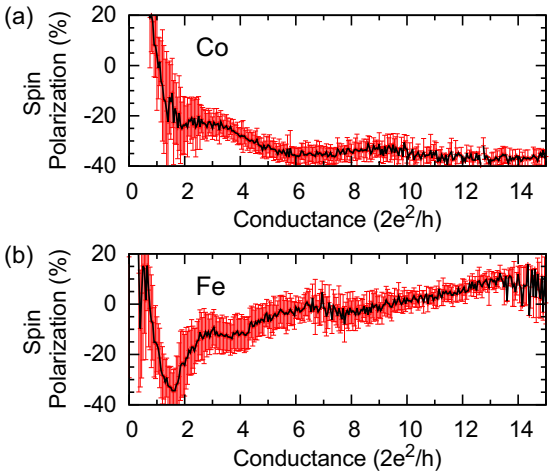

FIG. 13. Computed spin polarization of the current as a function of the conductance for Co (a) and Fe (b). The solid lines correspond to the average value and the bars to the standard deviation.

APPENDIX: SOME ADDITIONAL THEORETICAL RESULTS FOR Co AND Fe CONTACTS

For completeness, we display in Fig. 12 our theoretical results for the Fano factor and the spin-resolved channel distributions for the Co and Fe contacts. As explained in the main text, these results are qualitatively similar to those of Ni and confirm the general conclusions drawn on the nature of the transport properties of ferromagnetic atomic contacts. We also show in Figs. 13(a) and 13(b) the corresponding results for the current spin polarization in Co and Fe contacts. Notice that the Co case is very similar to the Ni (Fig. 11), while in the Fe case the current spin polarization exhibits a sign change as a function of the contact size and it adopts rather small values for large contacts. An analysis of the channel distribution for Fe, see Figs. 12(e) and 12(f), suggests that this behavior is due to a reduced contribution of the minority-spin d bands, as compared with the other two ferromagnetic metals. Another feature in these results that is worth remarking is the fact that, as in the Ni case, the fluctuations in the current polarization are particularly large in the tunnel regime ($G < 1G_0$), when the contacts are already broken.

[1] N. Agraït, A. L. Yeyati, and J. M. van Ruitenbeek, Phys. Rep. **377**, 81 (2003).
[2] E. Scheer, N. Agraït, J. C. Cuevas, A. L. Yeyati, B. Ludoph, A. Martín-Rodero, G. Rubio, J. M. van Ruitenbeek, and C. Urbina, Nature (London) **394**, 154 (1998).
[3] H. E. van den Brom and J. M. van Ruitenbeek, Phys. Rev. Lett. **82**, 1526 (1999).
[4] P. J. Wheeler, J. Russom, K. Evans, N. King, and D. Natelson, Nano Lett. **10**, 1287 (2010).
[5] R. Chen, P. J. Wheeler, and D. Natelson, Phys. Rev. B **85**, 235455 (2012).
[6] M. Kumar, R. Avriller, A. L. Yeyati, and J. M. van Ruitenbeek, Phys. Rev. Lett. **108**, 146602 (2012).
[7] R. Vardimon, M. Klionsky, and O. Tal, Phys. Rev. B **88**, 161404 (2013).
[8] R. Chen, M. Matt, F. Pauly, P. Nielaba, J. C. Cuevas, and D. Natelson, J. Phys.: Condens. Matter **26**, 474204 (2014).

[9] B. Ludoph and J. M. van Ruitenbeek, Phys. Rev. B **59**, 12290 (1999).

[10] M. Tsutsui, T. Morikawa, A. Arima, and M. Taniguchi, Sci. Rep. **3**, 3326 (2013).

[11] C. Evangeli, M. Matt, L. Rincón-García, F. Pauly, P. Nielaba, G. Rubio-Bollinger, J. C. Cuevas, and N. Agraït, Nano Lett. **15**, 1006 (2015).

[12] R. H. M. Smit, C. Untiedt, and J. M. van Ruitenbeek, Nanotechnology **15**, S472 (2004).

[13] W. Lee, K. Kim, W. Jeong, L. A. Zotti, F. Pauly, J. C. Cuevas, and P. Reddy, Nature (London) **498**, 209 (2013).

[14] K. I. Bolotin, F. Kuemmeth, and D. C. Ralph, Phys. Rev. Lett. **97**, 127202 (2006).

[15] A. Sokolov, E. Y. Tsymbal, J. Redepenning, and B. Doudin, Nat. Nanotechnol. **2**, 171 (2007).

[16] N. Néel, J. Kröger, and R. Berndt, Phys. Rev. Lett. **102**, 086805 (2009).

[17] S. Egle, C. Bacca, H.-F. Pernau, M. Hüfner, D. Hinzke, U. Nowak, and E. Scheer, Phys. Rev. B **81**, 134402 (2010).

[18] F. Strigl, C. Espy, M. Bückle, E. Scheer, and T. Pietsch, Nat. Commun. **6**, 6172 (2015).

[19] R. Vardimon, M. Klionsky, and O. Tal, Nano Lett. **15**, 3894 (2015).

[20] N. F. Mott, Proc. R. Soc. London, Ser. A **153**, 699 (1936).

[21] N. F. Mott and H. Jones, *The Theory of the Properties of Metals and Alloys* (Oxford University Press, London, 1936).

[22] Z. Jin, A. Tkach, F. Casper, V. Spetter, H. Grimm, A. Thomas, T. Kampfrath, M. Bonn, M. Kläui, and D. Turchinovich, Nat. Phys. **11**, 761 (2015).

[23] C. Sirvent, J. G. Rodrigo, S. Vieira, L. Jurczyszyn, N. Mingo, and F. Flores, Phys. Rev. B **53**, 16086 (1996).

[24] J. L. Costa-Krämer, Phys. Rev. B **55**, R4875 (1997).

[25] K. Hansen, E. Laegsgaard, I. Stensgaard, and F. Besenbacher, Phys. Rev. B **56**, 2208 (1997).

[26] F. Ott, S. Barberan, J. G. Lunney, J. M. D. Coey, P. Berthet, A. M. de Leon-Guevara, and A. Revcolevschi, Phys. Rev. B **58**, 4656 (1998).

[27] H. Oshima and K. Miyano, Appl. Phys. Lett. **73**, 2203 (1998).

[28] T. Ono, Y. Ooka, H. Miyajima, and Y. Otani, Appl. Phys. Lett. **75**, 1622 (1999).

[29] F. Komori and K. Nakatsuji, J. Phys. Soc. Jpn. **68**, 3786 (1999).

[30] N. García, M. Muñoz, and Y.-W. Zhao, Phys. Rev. Lett. **82**, 2923 (1999).

[31] B. Ludoph and J. M. van Ruitenbeek, Phys. Rev. B **61**, 2273 (2000).

[32] A. I. Yanson, Ph.D. thesis, Universiteit Leiden, 2001.

[33] M. Viret, S. Berger, M. Gabureac, F. Ott, D. Olligs, I. Petej, J. F. Gregg, C. Fermon, G. Francinet, and G. Le Goff, Phys. Rev. B **66**, 220401(R) (2002).

[34] F. Elhoussine, S. Mátéfi-Tempfli, A. Encinas, and L. Piraux, Appl. Phys. Lett. **81**, 1681 (2002).

[35] M. Shimizu, E. Saitoh, H. Miyajima, and Y. Otani, J. Magn. Magn. Mater. **239**, 243 (2002).

[36] D. Gillingham, I. Linington, and J. Bland, J. Phys.: Condens. Matter **14**, L567 (2002).

[37] V. Rodrigues, J. Bettini, P. C. Silva, and D. Ugarte, Phys. Rev. Lett. **91**, 096801 (2003).

[38] D. Gillingham, C. Müller, and J. Bland, J. Phys.: Condens. Matter **15**, L291 (2003).

[39] D. Gillingham, I. Linington, C. Müller, and J. Bland, J. Appl. Phys. **93**, 7388 (2003).

[40] C. Untiedt, D. M. T. Dekker, D. Djukic, and J. M. van Ruitenbeek, Phys. Rev. B **69**, 081401(R) (2004).

[41] M. Gabureac, M. Viret, F. Ott, and C. Fermon, Phys. Rev. B **69**, 100401(R) (2004).

[42] C.-S. Yang, C. Zhang, J. Redepenning, and B. Doudin, Appl. Phys. Lett. **84**, 2865 (2004).

[43] J. L. Costa-Krämer, M. Díaz, and P. A. Serena, Appl. Phys. A **81**, 1539 (2005).

[44] K. I. Bolotin, F. Kuemmeth, A. N. Pasupathy, and D. C. Ralph, Nano Lett. **6**, 123 (2006).

[45] Z. K. Keane, L. H. Yu, and D. Natelson, Appl. Phys. Lett. **88**, 062514 (2006).

[46] M. Viret, M. Gabureac, F. Ott, C. Fermon, C. Barreteau, G. Autés, and R. Guirardo-Lopez, Eur. Phys. J. B **51**, 1 (2006).

[47] M. R. Calvo, J. Fernández-Rossier, J. J. Palacios, D. Jacob, D. Natelson, and C. Untiedt, Nature (London) **458**, 1150 (2009).

[48] A. Halbritter, P. Makk, Sz. Mackowiak, Sz. Csonka, M. Wawrzyniak, and J. Martinek, Phys. Rev. Lett. **105**, 266805 (2010).

[49] Y. Moriguchi, K. Yamauchi, S. Kurokawa, and A. Sakai, Surf. Sci. **606**, 928 (2012).

[50] A. von Bieren, A. K. Patra, S. Krzyk, J. Rhensius, R. M. Reeve, L. J. Heyderman, R. Hoffmann-Vogel, and M. Kläui, Phys. Rev. Lett. **110**, 067203 (2013).

[51] J. Velev, R. F. Sabirianov, S. S. Jaswal, and E. Y. Tsymbal, Phys. Rev. Lett. **94**, 127203 (2005).

[52] M. Häfner, J. K. Viljas, and J. C. Cuevas, Phys. Rev. B **79**, 140410(R) (2009).

[53] S.-F. Shi and D. C. Ralph, Nat. Nanotechnol. **2**, 522 (2007).

[54] S.-F. Shi, K. I. Bolotin, F. Kuemmeth, and D. C. Ralph, Phys. Rev. B **76**, 184438 (2007).

[55] J. C. Cuevas, A. Levy Yeyati, and A. Martin-Rodero, Phys. Rev. Lett. **80**, 1066 (1998).

[56] A. Martín-Rodero, A. Levy Yeyati, and J. C. Cuevas, Physica C **352**, 67 (2001).

[57] P. S. Krstić, X.-G. Zhang, and W. H. Butler, Phys. Rev. B **66**, 205319 (2002).

[58] A. Smogunov, A. Dal Corso, and E. Tosatti, Surf. Sci. **507-510**, 609 (2002); **532-535**, 549 (2003).

[59] A. Delin and E. Tosatti, Phys. Rev. B **68**, 144434 (2003).

[60] J. Velev and W. H. Butler, Phys. Rev. B **69**, 094425 (2004).

[61] A. Bagrets, N. Papanikolaou, and I. Mertig, Phys. Rev. B **70**, 064410 (2004).

[62] A. R. Rocha and S. Sanvito, Phys. Rev. B **70**, 094406 (2004).

[63] D. Jacob, J. Fernández-Rossier, and J. J. Palacios, Phys. Rev. B **71**, 220403(R) (2005).

[64] M. Wierzbowska, A. Delin, and E. Tosatti, Phys. Rev. B **72**, 035439 (2005).

[65] H. Dalgleish and G. Kirczenow, Phys. Rev. B **72**, 155429 (2005).

[66] P. A. Khomyakov, G. Brocks, V. Karpan, M. Zwierzycki, and P. J. Kelly, Phys. Rev. B **72**, 035450 (2005).

[67] J. Fernández-Rossier, D. Jacob, C. Untiedt, and J. J. Palacios, Phys. Rev. B **72**, 224418 (2005).

[68] A. Smogunov, A. Dal Corso, and E. Tosatti, Phys. Rev. B **73**, 075418 (2006).

[69] F. Pauly, M. Dreher, J. K. Viljas, M. Häfner, J. C. Cuevas, and P. Nielaba, Phys. Rev. B **74**, 235106 (2006).
[70] D. Jacob and J. J. Palacios, Phys. Rev. B **73**, 075429 (2006).
[71] G. Autés, C. Barreteau, D. Spanjaard, and M. C. Desjonqures, J. Phys.: Condens. Matter **18**, 6785 (2006).
[72] K. Xia, M. Zwierzycki, M. Talanana, P. J. Kelly, and G. E. W. Bauer, Phys. Rev. B **73**, 064420 (2006).
[73] A. R. Rocha, T. Archer, and S. Sanvito, Phys. Rev. B **76**, 054435 (2007).
[74] J. C. Tung and G. Y. Guo, Phys. Rev. B **76**, 094413 (2007).
[75] A. Bagrets, N. Papanikolaou, and I. Mertig, Phys. Rev. B **75**, 235448 (2007).
[76] G. Autés, C. Barreteau, M.-C. Desjonquères, D. Spanjaard, and M. Viret, Europhys. Lett. **83**, 17010 (2008).
[77] D. Jacob, J. Fernández-Rossier, and J. J. Palacios, Phys. Rev. B **77**, 165412 (2008).
[78] K. Tao, I. Rungger, S. Sanvito, and V. S. Stepanyuk, Phys. Rev. B **82**, 085412 (2010).
[79] B. Hardrat, N.-P. Wang, F. Freimuth, Y. Mokrousov, and S. Heinze, Phys. Rev. B **85**, 245412 (2012).
[80] Y.-q. Xie, Q. Li, L. Huang, X. Ye, and S.-H. Ke, Appl. Phys. Lett. **101**, 192408 (2012).
[81] M. R. Calvo, D. Jacob, and C. Untiedt, Phys. Rev. B **86**, 075447 (2012).
[82] Z. Y. Tan, X.-l. Zheng, X. Ye, Y.-q. Xie, and S.-H. Ke, J. Appl. Phys. **114**, 063711 (2013).
[83] E. Scheer, P. Joyez, D. Esteve, C. Urbina, and M. H. Devoret, Phys. Rev. Lett. **78**, 3535 (1997).
[84] C. J. Muller, J. M. van Ruitenbeek, and L. J. de Jongh, Phys. Rev. Lett. **69**, 140 (1992).
[85] M. Dreher, F. Pauly, J. Heurich, J. C. Cuevas, E. Scheer, and P. Nielaba, Phys. Rev. B **72**, 075435 (2005).
[86] F. Pauly, J. K. Viljas, M. Bürkle, M. Dreher, P. Nielaba, and J. C. Cuevas, Phys. Rev. B **84**, 195420 (2011).
[87] C. Schirm, M. Matt, F. Pauly, J. C. Cuevas, P. Nielaba, and E. Scheer, Nat. Nanotechnol. **8**, 645 (2013).
[88] S. Plimpton, J. Comput. Phys. **117**, 1 (1995).
[89] See http://lammps.sandia.gov.
[90] H. W. Sheng, M. J. Kramer, A. Cadien, T. Fujita, and M. W. Chen, Phys. Rev. B **83**, 134118 (2011).
[91] G. P. Purja Pun and Y. Mishin, Phys. Rev. B **86**, 134116 (2012).
[92] M. I. Mendelev, S. Han, D. J. Srolovitz, G. J. Ackland, D. Y. Sun, and M. Asta, Philos. Mag. A **83**, 3977 (2003).
[93] D. Frenkel and B. Smit, *Understanding Molecular Simulation* (Academic Press, San Diego, 2004).
[94] M. J. Mehl and D. A. Papaconstantopoulos, Phys. Rev. B **54**, 4519 (1996).
[95] M. J. Mehl and D. A. Papaconstantopoulos, *Computational Materials Science*, edited by C. Fong (World Scientific, Singapore, 1998).
[96] N. C. Bacalis, D. A. Papaconstantopoulos, M. J. Mehl, and M. Lach-hab, Physica B **296**, 125 (2001).
[97] F. Guinea, C. Tejedor, F. Flores, and E. Louis, Phys. Rev. B **28**, 4397 (1983).
[98] F. Pauly, J. K. Viljas, U. Huniar, M. Häfner, S. Wohlthat, M. Bürkle, J. C. Cuevas, and G. Schön, New J. Phys. **10**, 125019 (2008).
[99] J. C. Cuevas and E. Scheer, *Molecular Electronics: An Introduction to Theory and Experiment* (World Scientific, Singapore, 2010).
[100] G. Rubio, N. Agrait, and S. Vieira, Phys. Rev. Lett. **76**, 2302 (1996).
[101] Yu. V. Sharvin, Sov. Phys. JETP **21**, 655 (1965) [Zh. Eksp. Teor. Fiz. **48**, 984 (1965)].
[102] Y. M. Blanter and M. Büttiker, Phys. Rep. **336**, 1 (2000).
[103] H. E. van den Brom, *Noise Properties of Atomic-Size Contacts* (Universiteit Leiden, 2000).
[104] K. E. Nagaev, Phys. Lett. A **169**, 103 (1992).
[105] C. W. J. Beenakker and M. Büttiker, Phys. Rev. B **46**, 1889 (1992).
[106] O. N. Dorokhov, JETP Lett. **36**, 318 (1982).
[107] C. W. J. Beenakker, Rev. Mod. Phys. **69**, 731 (1997).
[108] R. Meservey and P. M. Tedrow, Phys. Rep. **238**, 173 (1994).
[109] J. Bürki, C. A. Stafford, X. Zotos, and D. Baeriswyl, Phys. Rev. B **60**, 5000 (1999).
[110] J. Bürki and C. A. Stafford, Phys. Rev. Lett. **83**, 3342 (1999).
[111] C. W. J. Beenakker and J. A. Melsen, Phys. Rev. B **50**, 2450 (1994).
[112] J. J. Riquelme, L. de la Vega, A. Levy Yeyati, N. Agraït, A. Martin-Rodero, and G. Rubio-Bollinger, Europhys. Lett. **70**, 663 (2005).
[113] D. Erts, H. Olin, L. Ryen, E. Olsson, and A. Thölén, Phys. Rev. B **61**, 12725 (2000).
[114] M. J. M. de Jong and C. W. J. Beenakker, Phys. Rev. B **51**, 16867 (1995).